Elsevier Editorial System(tm) for Energy and Buildings
Manuscript Draft

Manuscript Number: ENB-D-13-00108R2

Title: Modeling and Experimental Validation of a Solar-Assisted Direct Expansion Air Conditioning System

Article Type: Full Length Article

Keywords: energy saving, solar-assisted air conditioner, modeling, experimental validation, performance prediction.

Corresponding Author: Prof. Quang Ha, PhD

Corresponding Author's Institution: University of Technology Sydney

First Author: Vahid Vakiloroaya

Order of Authors: Vahid Vakiloroaya; Quang Ha, PhD; Miroslaw Skibniewski, PhD

Abstract: Continuous increase in global electricity consumption, environmental hazards of pollution and depletion of fossil fuel resources have brought about a paradigm shift in the development of eco-friendly and energy-efficient technologies. This paper reports on an experimental study to investigate the inherent operational characteristics of a new direct-expansion air conditioning system combined with a vacuum solar collector. Mathematical models of the system components are firstly derived and then validated against experimental results. To investigate the potential of energy savings, the hybrid solar-assisted air-conditioner is installed and extensively equipped with a number of sensors and instrumentation devices, for experimentation and data collection. The influence on the system energy usage of the average water temperature, storage tank size and room set-point temperature are then analyzed. Once the air-conditioned room has achieved its desired temperature, the compressor turns off while the cooling process still continues until the refrigerant pressure no longer maintains the desired temperature. The advantages of the proposed hybrid system rest with the fact that the compressor can remain off in a longer period by heat impartation into the refrigerant via the water storage tank. Results show an average monthly energy saving of about between 25% and 42%.

*Manuscript
Click here to view linked References

Modeling and Experimental Validation of a Solar-Assisted Direct Expansion Air Conditioning System

VahidVakiloroaya[a], Q.P.Ha[a,*] and M. Skibniewski[b]

[a]School of Electrical, Mechanical and Mechatronic Systems, University of Technology Sydney, Australia

[b]A.J. Clark School of Engineering, University of Maryland, USA

* Corresponding author, E-mail address: quang.ha@uts.edu.au

Abstract

Continuous increase in global electricity consumption, environmental hazards of pollution and depletion of fossil fuel resources have brought about a paradigm shift in the development of eco-friendly and energy-efficient technologies. This paper reports on an experimental study to investigate the inherent operational characteristics of a new direct-expansion air conditioning system combined with a vacuum solar collector. Mathematical models of the system components are firstly derived and then validated against experimental results. To investigate the potential of energy savings, the hybrid solar-assisted air-conditioner is installed and extensively equipped with a number of sensors and instrumentation devices, for experimentation and data collection. The influence on the system energy usage of the average water temperature, storage tank size and room set-point temperature are then analyzed. Once the air-conditioned room has achieved its desired temperature, the compressor turns off while the cooling process still continues until the refrigerant pressure no longer maintains the desired temperature. The advantages of the proposed hybrid system rest with the fact that the compressor can remain off in a longer period by heat impartation into the refrigerant via the water storage tank. Results show an average monthly energy saving of about between 25% and 42%.

Keywords: energy saving, solar-assisted air conditioner, modeling, experimental validation, performance prediction.

Nomenclature

A	cross-sectional area (m^2)	Subscripts	
C_p	heat capacity (kJ/(kg°C))		
D_i	inside diameter of tube (m)	*a*	air
D_o	outside diameter of tube (m)	*c*	condenser
h	enthalpy (kJ/kg)	*cap*	capillary tube
I_t	total solar radiation (kW/m^2)	*comp*	compressor
k	polytropic index of the refrigerant vapor	*c*	condenser
L	length (m)	*col*	collector
$\dot{m}$	refrigerant mass flow rate (kg/s)	*ds*	de-superheat
M	mass (kg)	*e*	evaporator
p_c	condenser pressure (kPa)	*f*	water inside storage tank
p_e	evaporator pressure (kPa)	*g*	saturated vapor
T	temperature (°C)	*hx*	heat exchanger
t	time (min)	*i*	inlet
U	overall heat loss coefficient ($kW/(m^2°C)$)	*int*	interface
V_D	displacement volume of the compressor (m^3/s)	*l*	saturated liquid
W_{in}	electrical power consumption of the compressor (kW)	*o*	outlet
α_i	heat transfer coefficient between tube wall and refrigerant ($kW/(m^2$ °C))	*r*	refrigerant
α_o	heat transfer coefficient between tube wall and air ($kW/(m^2$ °C))	*sc*	subcool
α_s	collector absorptance value	*sh*	superheat
$\bar{\gamma}$	mean value of void fraction	*t*	tank
η_{comp}	total efficiency of the compressor	*tp*	two-phase
η_v	volumetric efficiency of the compressor	*w*	wall
ϑ_{suc}	specific volume at the compressor inlet (m^3/kg)		
τ_s	collector transmittance value		
ρ	density (kg/m^3)		

1. Introduction

Growing demand for heating, ventilating and air conditioning (HVAC) systems has nowadays imposed a considerable increase in electricity, which represents approximately 50% of total building energy consumption [1].For air conditioning, one commonly-used type of HVAC systems is the direct expansion (DX) wall-mounted air-conditioner with a vapor compression cycle. When compared to the chilled water based air conditioning systems, the use of DX systems is more advantageous due to simpler operation and less maintenance cost [2-5]. While this system is energy-efficient and highly comfortable for residential and commercial buildings in different types of climatic conditions, their

combination with free energy sources in order to reduce the power consumption has been an interesting topic for researchers. In fact, as the typical value of coefficient of performance (COP) for vapor compression systems is between 2 to 3 [6], combining these systems with any type of renewable energy resources can certainly increase their COP. To this end, it has been found that the electric compression and absorption systems have very high energy saving potential when utilizing the availability of solar energy [7].

Among different types of renewable source of energy available, solar thermal energy is abundantly present and environmentally sustainable. Advantages include significant reductions in energy usage as well as ozone depletion (ODP), and smaller contribution to greenhouse effects and lower CO_2 emission compared to electrically-operated plants. These have therefore promoted the design alternative of using solar collectors for HVAC systems [8-10]. Over the past decade, investigation has been carried out on the feasibility and energy saving potential of different hybrid air conditioning systems [11-14]. Bilgili [15] proposed a solar electric-vapor compression refrigeration system and investigated its performance for different evaporating temperatures, nevertheless without considering the cost of photovoltaic solar panels. A solar-assisted ejector cooling/heating system was developed by Huang et al. [16], wherein the solar ejector cooling system was connected to a conventional inverter type air conditioner to reduce the condensing temperature and hence increase the system COP. Fong et al. [7] proposed a solar hybrid air conditioning system using adsorption refrigeration, chilled ceiling and desiccant dehumidification. Their simulation results showed that the proposed system can satisfy the necessary indoor conditions for office use with a year-round primary energy usage up to 47.3%lower than consumption of a conventional air conditioning system. However, the system would be quite expensive and suitable only for large buildings. A hybrid solar-assisted air conditioner has been recently developed in Al-Alili et al. [17], consisting of a solid desiccant wheel cycle and a conventional vapor compression cycle. Their results showed that the COP of the proposed solar-assisted plant is higher than that of a vapor compression cycle powered by photovoltaic panels and a solar absorption cycle. However, as solar thermal energy is obviously more efficient than photovoltaics in HVAC, research effort has been devoted to its use in hybrid air-conditioning for further improving the system energy efficiency and COP. Modeling and control of such systems

remain of an increasing interest. For this purpose, a synergetic framework of system identification, empirical modeling, optimization and control has been proposed [18,19]. In this new hybrid solar system, in addition to a conventional compressor used to increase the pressure on the gas, forcing it into a liquid in the condenser coil, a hot water storage tank integrated with a vacuum solar collector is installed after the compressor to supply superheat to the refrigerant and increase its kinetic energy. A larger condenser is used to reject the additional heat obtained from the water storage tank. Therefore, when the room temperature achieves its desired set-point, the compressor will turn off and the additional refrigerant temperature resulting from the hot water storage tank will help it to stay off longer. This method reduces the compressor duty cycle, while fulfilling the building cooling demand, to eventually result in overall energy saving. It is observed that there has been to date no reported research work on comprehensive modeling and experimental validation for the performance of a hybrid solar DX air-conditioner where a solar thermal collector is installed after its compressor.

In this paper, the objectives are to develop reliable mathematical models for components of a direct expansion solar-assisted DX air-conditioner with solar thermal collectors being installed after its compressor, and validate them experimentally via their thermal performance. To this end, mathematical models based on dynamic heat transfer through the system components are developed and incorporated into a transient computer tool, TRNSYS [20], using FORTRAN codes. An iterative numerical procedure is implemented to solve simultaneously heat transfer equations for various components of the system. Experimental results are then compared with simulation prediction to validate the system's mathematical models. A key element of this work is to monitor the system performance in order to quantify energy saving potential for optimal usage of the system. Parametric study of the system has also been performed to understand the influence of the principal parameters of the system on its performance. For this purpose, the system is extensively equipped with sensors and several data logger devices to record its performance data over time. The system is operated over a wide range of climatic conditions for two typical summer weeks. Results showed monthly average energy saving of 25% to42%, compared to the energy consumption of a conventional air-conditioner.

The remainder of the paper is organized as follows. After the introduction, Section 2 presents the system description and details the component-wise models of the system. The experimental test rig

and model validation are described in Section 3. Results and discussion are given in Section 4. Finally a conclusion is drawn in Section 5.

2. System Modeling

This section describes the system configuration and derives mathematical models for its components.

2.1 System Configuration

The single-stage vapor compression solar air-conditioner consists of six major components: a compressor, an air-cooled condenser, an expansion device, a DX evaporator, a solar vacuum collector and a hot water storage tank. The schematic diagram of the arrangement is shown in Fig. 1. The cycle starts with a mixture of liquid and vapor refrigerant entering the evaporator (point 1). The heat from the warm air is absorbed by the evaporator coil. During this process, the state of the refrigerant is changed from liquid to gas and becomes superheated at the evaporator exit. The superheat vapor enters the compressor (point 2), where the increasing pressure raises the refrigerant temperature. A vacuum solar panel installed after the compressor uses solar radiation to heat up the water. An insulated water storage tank is connected to the vacuum solar collector to maintain the water temperature. The refrigerant from the compressor goes through the copper coil inside the tank for heat exchanges (point 3).When the air-conditioned room reaches its desired set-point temperature, the compressor turns off. This additional kinetic energy helps it to stay off longer, thus reducing its duty cycle and hence increasing the system average COP. However, during the compressor's operation time in full load conditions, additional heat absorbed by the refrigerant in the water storage tank needs to be rejected in the condenser, thus requiring a slightly larger condenser area. This will be discussed later in the section on energy analysis.

After the storage tank, a further temperature reduction takes place in the condenser and causes it to de-superheat (point 4); thus, the refrigerant liquid is sub-cooled as it enters the expansion device (point 5). Sub-cooling prevents flash gas formation before the expansion device and increases the evaporator's refrigeration effect. The high pressure sub-cooled refrigerant flows through the capillary

tube, which reduces both its pressure and temperature.

2.2 DX Evaporator

By considering the thermodynamic states of the refrigerant, the evaporator can be divided into two zones: a liquid-vapor mixture (two-phase) zone and a superheated vapor (single-phase) zone, as shown in Fig. 2.This model does not include condensation on the external surface of the evaporator. In the two-phase zone, the refrigerant temperature is at its saturated value without spatial variations. In the superheated zone, the refrigerant's temperature increases as it travels from the two-phase vapor interface toward the evaporator outlet. In this section, by applying the energy and mass balance for each zone, the lumped-parameter moving-boundary model is developed to describe the dynamics of the DX evaporator. The energy balance equation for the two-phase zone is as:

$$A_e L_{e,tp}\left(\frac{d(\rho_{e,l}h_{e,l})}{dt}(1-\bar{\gamma})+\frac{d(\rho_{e,g}h_{e,g})}{dt}\bar{\gamma}-\frac{dp_e}{dt}\right)+A_e(1-\bar{\gamma})(\rho_{e,l}h_{e,l}-\rho_{e,g}h_{e,g})\frac{dL_{e,tp}}{dt}= \tag{1}$$
$$\dot{m}_{e,i}h_{e,i}-\dot{m}_{e,\mathrm{int}}h_{e,g}+\alpha_{i,e,tp}\pi D_{e,i}L_{e,tp}(T_{e,tp,w}-T_{e,tp,r}),$$

where $L_{e,tp}$ denotes the length of the two-phase zone and varies with time due to any change in boundary conditions. The mass balance equation for the two-phase zone can be expressed as:

$$A_e L_{e,tp}\frac{d\rho_{e,tp}}{dp_e}\frac{dp_e}{dt}+A_e(\rho_{e,tp}-\rho_{e,g})\frac{dL_{e,tp}}{dt}=\dot{m}_{e,i}-\dot{m}_{e,\mathrm{int}}, \tag{2}$$

Where $\rho_{e,tp}$ is the average density of the refrigerant and can be determined as:

$$\rho_{e,tp}=\rho_{e,l}(1-\bar{\gamma})+\rho_{e,g}\bar{\gamma}. \tag{3}$$

The energy balance equation for the tube wall of the two-phase zone is:

$$C_{p,w}\rho_w A_w\frac{dT_{e,tp,w}}{dt}=\alpha_{i,e,tp}\pi D_{e,i}(T_{e,tp,r}-T_{e,tp,w})+\alpha_{o,e}\pi D_{e,o}(T_{e,a}-T_{e,tp,w}). \tag{4}$$

The energy balance equation for the vapor superheating zone is written as:

$$A_e L_{e,sh}\left(\rho_{sh}\frac{dh_{e,sh}}{dt}-\frac{dp_e}{dt}\right)=$$
$$\alpha_{i,e,sh}\pi D_{e,i}L_{e,sh}(T_{e,sh,w}-T_{e,sh,r})-(\dot{m}_{e,\mathrm{int}}-\rho_{e,g}A_e\frac{dL_{e,sh}}{dt})\frac{h_{e,o}-h_{e,g}}{2}-\dot{m}_{e,o}\frac{h_{e,o}-h_{e,g}}{2}. \quad (5)$$

The mass balance equation for the superheating zone is given by:

$$A_e L_{e,sh}\frac{d\rho_{e,sh}}{dt}+A_e(\rho_{e,g}-\rho_{e,sh})\frac{dL_{e,tp}}{dt}=\dot{m}_{e,\mathrm{int}}-\dot{m}_{e,o}. \quad (6)$$

Finally, the energy balance equation for the tube wall of the superheated zone can be expressed as:

$$(C_{p,w}\rho_w A_w)\left(\frac{dT_{e,sh,w}}{dt}+\frac{T_{e,tp,w}-T_{e,sh,w}}{L_{e,sh}}\frac{dL_{e,tp}}{dt}\right)=$$
$$\alpha_{i,e,sh}\pi D_{e,i}(T_{e,sh,r}-T_{e,sh,w})+\alpha_{o,e}\pi D_{e,o}(T_{e,a}-T_{e,sh,w}). \quad (7)$$

2.3 Air-Cooled Condenser

According to the phase of the refrigerant, the condenser operation can be divided into three zones: de-superheating, two-phase (a liquid-vapor) and subcooled liquid, as shown in Fig. 3. We assume that the pressure drop along the condenser tube compared with the total pressure head is negligible. The refrigerant that enters the condenser after leaving the water storage tank is then superheated. In the de-superheating zone the refrigerant temperature decreases as it travels from the condenser inlet towards the vapor/two-phase interface. The energy balance equation in this zone is given in the following equation:

$$A_c L_{c,ds}\left(\rho_{c,ds}\frac{dh_{c,g}}{dt}-\frac{dp_c}{dt}\right)=$$
$$\alpha_{i,c,ds}\pi D_{c,i}L_{c,ds}(T_{c,ds,w}-T_{c,ds,r})-\frac{1}{2}(\dot{m}_{c,i}+\dot{m}_{c,\mathrm{int},ds}-\rho_{c,g}A_c\frac{dL_{c,ds}}{dt})(h_{c,g}-h_{c,i}), \quad (8)$$

Where $L_{c,ds}$is the length of the de-superheating zone. The mass balance equation for this zone can be presented as:

$$A_c L_{c,ds} \frac{d\rho_{c,ds}}{dt} + A_c(\rho_{c,ds} - \rho_{c,g}) \frac{dL_{c,ds}}{dt} = \dot{m}_{c,i} - \dot{m}_{c,\text{int},ds}. \quad (9)$$

The energy balance equation for the tube wall of the de-superheating zone is given by:

$$(C_{p,w}\rho_w A_w)\left(\frac{dT_{c,ds,w}}{dt} + \frac{T_{c,ds,w} - T_{c,tp,w}}{L_{sp}} \frac{dL_{c,tp}}{dt}\right) =$$

$$\alpha_{i,c,ds}\pi D_{c,i}(T_{c,ds,r} - T_{c,ds,w}) + \alpha_{o,c}\pi D_{c,o}(T_{c,a} - T_{c,ds,w}). \quad (10)$$

In the two-phase zone, the refrigerant temperature without spatial variations is at its saturated value. The energy balance equation for the two-phase zone in the condenser is therefore:

$$A_c L_{c,tp}\left(\frac{d(\rho_{c,l}h_{c,l})}{dt}(1-\bar{\gamma}) + \frac{d(\rho_{c,g}h_{c,g})}{dt}\bar{\gamma} - \frac{dp_c}{dt}\right) + A_c(\rho_{c,g}h_{c,g} - \rho_{c,l}h_{c,l})\frac{dL_{c,ds}}{dt} +$$

$$A_c\bar{\gamma}(\rho_{c,g}h_{c,g} - \rho_{c,l}h_{c,l})\frac{dL_{c,tp}}{dt} = \dot{m}_{c,i}h_{c,i} - \dot{m}_{c,\text{int}}h_g + \alpha_{i,c,tp}\pi D_{c,i}L_{c,tp}(T_{c,tp,w} - T_{c,tp,r}). \quad (11)$$

The mass balance equation of the two-phase zone is obtained as:

$$A_c L_{c,tp}\frac{d\rho_{c,tp}}{dp_c}\frac{dp_c}{dt} + A_c(\rho_{c,g} - \rho_{c,l})\frac{dL_{c,ds}}{dt} + A_c(\rho_{c,ds} - \rho_{c,l})\frac{dL_{c,tp}}{dt} = \dot{m}_{c,\text{int},ds} - \dot{m}_{c,\text{int},tp}, \quad (12)$$

where$\rho_{c,tp}$ is the average density of the refrigerant and can be determined as:

$$\rho_{c,tp} = \rho_{c,l}(1-\bar{\gamma}) + \rho_{c,g}\bar{\gamma}. \quad (13)$$

The energy balance equation at the tube wall of the two-phase zone is:

$$C_{p,w}\rho_w A_w \frac{dT_{c,tp,w}}{dt} = \alpha_{i,c,tp}\pi D_{c,i}(T_{c,tp,r} - T_{c,tp,w}) + \alpha_{o,c}\pi D_{c,o}(T_{c,a} - T_{c,tp,w}). \quad (14)$$

In the subcooled liquid zone, the temperature of refrigerant decreases as it travels from the two-phase/liquid interface towards the condenser outlet. The energy balance equation for thesubcooled liquid zone is thus:

$$A_e L_{c,sc}\left((\frac{\rho_{c,l}}{2}\frac{dh_{c,l}}{dp_c})\frac{dp_c}{dt}+\frac{\rho_{c,l}}{2}\frac{dh_{c,o}}{dt}\right)+A_c\rho_{c,l}\frac{(h_{c,l}-h_{c,o})}{2}(\frac{dL_{c,ds}}{dt}+\frac{dL_{c,tp}}{dt})=$$

$$\alpha_{i,c,sc}\pi D_{c,i}L_{c,sp}(T_{c,sp,w}-T_{c,sp,r})+\dot{m}_{c,o}(h_{c,l}-h_{c,o}). \quad (15)$$

The mass flow rate at the outlet is assumed to be equal to that in the tow-phase zone, i.e.,

$$\dot{m}_{c,\text{int},tp}=\dot{m}_{c,o}. \quad (16)$$

Finally, the energy balance the tube wall of the subcooled liquid zone is:

$$(C_{p,w}\rho_w A_w)\left(\frac{dT_{c,sc,w}}{dt}+\frac{T_{c,tp,w}-T_{c,sc,w}}{L_{c,sc}}(\frac{dL_{c,ds}}{dt}+\frac{dL_{c,tp}}{dt})\right)=$$

$$\alpha_{i,c,sc}\pi D_{c,i}(T_{c,sc,r}-T_{c,sc,w})+\alpha_{o,c}\pi D_{c,o}(T_{c,a}-T_{c,sc,w}). \quad (17)$$

2.4 Compressor

Since the electromechanical process of reaching the compressor operational speed is faster than the associated thermal process, its transient characteristics can be neglected [2] and modelled by just algebraic equations [21]. Therefore, the compressor is modelled with the use of an iterative procedure described by the refrigerant mass flow rate of the compressor, the polytropic work input to the compressor and the refrigerant enthalpy at the compressor exit. The compressor mass flow rate is given by:

$$\dot{m}_{r,comp}=\frac{V_D\eta_v}{v_{suc}}. \quad (18)$$

The input electric power to the compressor is given by:

$$W_{in}=\frac{\dot{m}_{r,comp}}{\eta_{comp}}p_e v_{suc}(\frac{k}{k-1})\left((\frac{p_c}{p_e})^{(\frac{k-1}{k})}-1\right). \quad (19)$$

Then, the refrigerant enthalpy leaving the compressor can be calculated as:

$$h_{r,o,comp} = \frac{\dot{m}_{r,comp} h_{r,i,comp} + W_{in}}{\dot{m}_{r,comp}}. \quad (20)$$

Finally, the refrigerant temperature leaving the compressor can be determined by using the compressor discharge pressure and enthalpy of the refrigerant leaving the compressor and by referring to the refrigerant thermodynamic properties in the superheating zone.

2.5 Water Storage Tank

The vacuum solar collector uses solar radiation to heat up the storage water. The solar collector for this project is a two-layered glass tube and the space in between the tubes is evacuated, creating a vacuum jacket. Therefore, there is a perfect insulation barrier, preventing heat loss due to convection and conduction. The selective coating is deposited onto the outside surface of a glass tubes domed at one end. The heat is then transferred from the storage water to an immersed heat exchanger, which passes through the storage tank. The refrigerant state at the immersed coil inlet is determined from the compressor model. For the solar storage tank with a coiled pipe used as a heat exchanger, it is assumed that the free flow for water is dependent on the temperature generated via the density difference, the water flow is laminar, and the storage water is only heated by the solar collected circuit. Thus, the energy balance for the water storage tank yields:

$$M_f C_{p,f} \frac{dT_f}{dt} = A_{col} I_t \tau_s \alpha_s + \dot{m}_r (h_{t,r,i} - h_{t,r,o}) + A_t U_t (T_a - T_f). \quad (21)$$

The energy balance principle for the immersed coil inside the storage tank gives:

$$T_{t,r,o} = T_f + (T_{t,r,i} - T_f) \exp(-\frac{A_{hx} U_{hx}}{\dot{m}_r C_{p,r}}). \quad (22)$$

2.6 Capillary Tube

The capillary tube is a constant area expansion device, commonly-used in small air conditioning system. For an isenthalpic process in the capillary tube, the following equation is given:

$$h_{r,i,cap} = h_{r,o,cap}, \quad (23)$$

where $h_{r,i,cap}$ and $h_{r,o,cap}$ are respectively the specific enthalpies of the refrigerant entering and leaving the capillary tube. Therefore, the temperature of the refrigerant leaving the capillary tube can be determined after calculating the refrigerant enthalpy and measuring the refrigerant pressure at the capillary tube exit.

3. Model Validation

This section describes the experimental test rig and the validation work for the mathematical models derived in the previous section.

3.1 Experimental Rig

Experimental work was carried out using a newly-developed solar-assisted DX hybrid air conditioner, shown in Fig. 4, as outlined in [18]. The experimental set-up is mainly composed of two parts: an air-conditioned room served by the direct expansion evaporator unit, and the condensing unit combined with a solar vacuum collector. The floor area of the air-conditioned room is 3 meter high and of 38 square meters in floor area. The nominal output cooling capacity of the air-conditioner is 6 kW. The plant has one hermetic rotary compressor of the scroll type using refrigerant R410A as a working fluid. The amount of charged refrigerant into the system is 1.8 kg. The design air flow rate of the evaporator fan is 850 m^3/h. The condenser is an air-cooled tube and uses a coated fin tube. The design air flow rate of the condenser axial fan is 2500 m^3/h and its rated power input is 50 W, which can be negligible as compared to the system's capacity of 6 kW. The collector is integrated at a tilted angle of 5° and oriented towards north (for usage in the southern hemisphere). The solar collector is made of 11 evacuated tubes with length 55 cm and diameter 10 cm. The solar collector is equipped with a 35-litre horizontal cylindrical storage tank, insulated by polyurethane of 55 mm thickness.

This system has been fully-instrumented to facilitate a number of tests under different operation conditions. High precision sensors/transducers are used for monitoring all operational variables. The following parameters are measured: meteorological parameters (global solar radiation, ambient temperature and ambient relative humidity), storage tank water temperature, indoor temperature and

relative humidity, temperature of the refrigerant entering and leaving water storage tank, compressor, condenser, evaporator and capillary tube, total power consumption of the plant, refrigerant suction and discharge pressure, and refrigerant pressure after the hot water storage tank. The global radiation is measured by means of a solarimeter of the type CR100-A, mounted on a surface parallel to the plane of the collector. The solarimeter is integrated to a computer based-KT250-AO data-logger. The outdoor temperature and relative humidity are measured by a combined sensor-data-logger devicewith a calibrated accuracy of ±0.4°C for temperature and ±2% for relative humidity. The measuring range for temperature is between -20°C and +70°C and from 5% and 95%for humidity. The sensor is integrated with a computer-based KT250-AO data-logger.

Six platinum resistance thermometers of the PT100 type are used with a calibrated accuracy of ±0.5°C for a temperature range from -50°C to +260°C to measure the refrigerant temperature before and after each component. These sensors are in direct contact with the refrigerant to achieve high accuracy. Another PT100 temperature sensor with the same specification is vertically-located inside the solar storage tank to measure the average temperature of the water inside the tank. Three pressure transducers with a calibrated accuracy of 1% are respectively installed in the suction line, the discharge line after the compressor and the discharge line after the storage tank. The measuring range for these pressure transducers located in the suction line is between 0 and 2000 kPa, and for pressure transducers located in the discharge lines is from 0 to 3500 kPa. All PT100 sensors and pressure transducers are integrated with a computer-based DT500 data-logger. The power of the air-conditioner is measured by a digital ac/dc power clamp multimeter of precision ±3.5%.

Field tests were run continuously to monitor the system performance at various weather conditions for two weeks. Day-long tests were carried out for 24 hours and all measured data was monitored in 10 minute intervals. All measurements were then computerized so that all the measured data could be recorded for subsequent analysis.

3.2 Simulation-Experimental Validation

Component-wise mathematical models are coded into the fully integrated visual interface known as TRNSYS simulation studio using FORTRAN for the validation purpose, combining the simulation

prediction and experimental monitoring approach, as adopted in [5]. Under the real world condition, there are many factors that influence on the system. In this study, all dimensions of the system components and connected pipes are included in the program. Experimentally collected data were entered through a dedicated visual interface. The simulation information flow diagram is shown in Fig.5, where the icon "building" represents the building information file created by PREBID and in compliance with the requirements of the ANSI/ASHRAE Standard 140-2007 [22]. The model includes a subroutine to evaluate the thermodynamic properties of refrigerant R410A. This simulation code is then used to calculate the main parameters such as temperatures of the refrigerant when leaving the DX evaporator, compressor, water storage tank, air-cooled condenser and capillary tube as well as the water temperature in the storage tank. The idea is to compare the behavior of the models with experimental responses as obtained from testing.

There are many parameters involved in the models which need validation. Some of these parameters can be measured directly and others should be calculated based on thermodynamic and heat transfer equations. The total length of both the evaporator and condenser were measured to include also the finned tubes. Saturation properties are considered as functions of pressure only. The mean void fraction appears to be invariant with respect to time. The compressor speed is 2830 rpm. The input parameters obtained via our simulation program are validated with measurements, as listed in Table 1.

3.3 Uncertainty and Error Analysis

Experimental studies usually involve some unpredictable and uncertain factors which occur due to instrumental manufacturing errors, calibration errors and human mistakes. These uncertainties should be treated by using a statistical approach. In this study, the non-dimensional deviation about the mean value was found for each reading from the following equation:

$$\varphi_i = \frac{y_{data,i} - y_{data,m}}{s_x}, \tag{24}$$

Where $y_{data,i}$ is the measured variables, $y_{data,m}$ is its average value,and the standard deviation s_x for a set

of N samples is determined by:

$$s_x = \sqrt{\frac{1}{N}\left(\sum_{i=1}^{N}(y_{data,i} - y_{data,m})^2\right)}, \quad (25)$$

$$y_{data,m} = \frac{1}{N}\sum_{i=1}^{N} y_{data,i}. \quad (26)$$

The value $\varphi_i$of each reading was compared with the ratio of the maximum allowable deviation from the mean value and the standard deviation.

For error analysis, the simulated performance of the system is compared with obtained experimental results. The simulation is run with a time interval of 10 minutes, i.e. equal to the monitoring time step in the real test process. This study uses the relative error (RE), the root mean square error (RMSE) and the coefficient of variance (CV) to indicate how well a regression model fits the observations. They are defined as follows:

$$RE = \frac{\sum_{i=1}^{N}\frac{\left|y_{pred,i} - y_{data,i}\right|}{y_{data,i}}}{N} \times 100\%, \quad (27)$$

$$RMSE = \sqrt{\frac{1}{N}\left(\sum_{i=1}^{N}(y_{pred,i} - y_{data,i})^2\right)}, \quad (28)$$

$$CV = \frac{RMSE}{y_{data,m}} \times 100\%, \quad (29)$$

Where $y_{pred,i}$ is the predicted variables. . For validation of the mathematical model, several field tests are run to cover a wide range of operating conditions. Simulation results of all validations found to be in good agreement with the experimental results, as shown in Figs. 6 to 11. Figure 6comparesthe predicted and experimental temperature of the refrigerant leaving the DX evaporator, wherein the deviation between experimental and predicted values falls within 9.57%. Figure 7 shows the plots of predicted and experimental values of the refrigerant's temperature leaving the compressor. It can be

seen that the model over predicted the experimental data by 11.4%. As shown in Fig. 8, the experimental temperature of the refrigerant leaving the water storage tank is deviated from the predicted values by 12.18%. The percentage deviation of the experimental and predicted values for the storage tank water temperature is 10.98%, as shown in Fig. 9. Figure 10depicts the comparison of the calculated and measured results for the temperature of the refrigerant leaving the condenser. The trend of the predicted results is similar to that obtained from experimental data. The calculated results are about 12.38% greater than the measured ones. Finally, Fig. 11 presents experimental and predicted values for refrigerant temperature leaving the capillary tube. It can be seen that the model over predicted the experimental data about 9.49%. Therefore, the mathematical models with accuracy being validated by using experimental data are ready to be used for system performance enhancement.

4. Results and Discussion

4.1 Test Scenario

To predict the system performance throughout the summer, which includes December, January and February in the southern hemisphere, the cooling load is calculated by using TRNSYS prior to the simulation process. The references for the indoor temperature and relative humidity during the cooling load calculation were set respectively at 23°C and 50%. The peak cooling load is estimated at 4.6 kW in the middle of February. The average temperature of the refrigerant entering and leaving the compressor are measured at16.6°C and 53.1°C, respectively. Similarly, the average refrigerant temperature at inlet and outlet of the air-cooled condenser are measured respectively as 61.2°C and 30°C. The temperature of the refrigerant leaving the water storage tank gets increased with an increase in solar intensity. The solar storage water tank, receiving solar energy from the collectors, is thermally insulated to allow the system to continuously operate even after three days of cool, cloudy weather. In addition, the cooler weather lowers the heat load, thereby increasing the temperature difference at the condenser and promoting more efficient heat transfer. On a sunny day, the water temperature can reach to between 75°C and85°C, depending on the solar radiation intensity and the ambient air dry-bulb temperature. On a heavily overcast day, the water temperature may vary from

70°C to 85°C. However, the average water temperature inside the storage tank is measured as 80.7°C. Monitored experimental data for the ambient dry bulb temperature and relative humidity are shown in Fig. 12 during two weeks of January, when the ambient temperature varied between 19°C and 33°C with an average temperature of 23.8°C. The average solar radiation intensity during two typical weeks was measured about 332 W/m^2.The first day of the period was a sunny day followed by three cloudy days. The three last days were again sunny days. The steady-state suction and discharge pressure at full load are measured respectively as 930 kPa and 2500 kPa. Moreover, simulation with TRNSYS 16 using "Meteonorm" can confirm more energy savings for a higher range of the ambient temperature.

4.2 Energy Analysis

In a vapor compression refrigeration cycle, the temperature of the refrigerant leaving the condenser highly affects the system performance [23]. On the other hand an increase of the subcool temperature by some centigrade degrees is desirable as it tends to increase the evaporator refrigeration effect. In the new HSAC, the temperature increase of the refrigerant entering the condenser is due to an additional input of heat by the water storage tank while the compressor is running. In this case, the temperature of the refrigerant leaving the condenser would increase which may reduce the subcool temperature and, in turn, decrease the system's COP. To solve this problem we used a slightly larger air-cooled condenser. Therefore, once the room has achieved its desired temperature, the compressor turns off while the room cooling process still continues until the refrigerant pressure within the circulation loop fails to maintain the desired temperature. The advantage of the proposed system is that heat can be imparted into the refrigerant via the water storage tank, so the compressor can remain off longer to increase the average COP. This is explained by the observation that while the compressor turns off, the temperature of the superheated gas increases in the hot water storage tank, more kinetic energy is generated in the gas molecules, and therefore, collisions between the molecules and the walls of the container take place more frequently and forcefully. As a result, when the room temperature achieves its desired amount, the compressor remains off longer since there is more kinetic energy for the refrigerant to be transferred from the high pressure zone to the low pressure zone. The room temperature eventually rises above the desired set-point temperature, which, in turn, triggers the

compressor to restart. Simulation results for November December, January, February and March showed that to support the building cooling load, the compressor of conventional plant had to operate for 763.2, 1108.8, 1209.6, 1152 and 979.2 minutes whilst it just needed around 441.6, 741.6, 907.2, 806.4 and 607.2 minutes, respectively, with the solar-assisted plant.

Although a slightly larger condenser (about less than 10% of its normal size) is required in full-load conditions to compensate for additional heat absorbed by the hot water storage tank, this size increase helps to raise the sub-cool temperature at the condenser outlet in partial load conditions. As the system operates mostly at partial loads, a higher sub-cooling temperature leads to less energy consumption by the compressor, which, more than offsetting the minor additional cost of manufacturing for this increase, eventually results in overall cost-effectiveness of the proposed system.

Since the system COP is much greater when the compressor is off than when it is on, the newly-configured air conditioner leads to a saving of (25-42)% of monthly average electrical energy as compared to a conventional system of equivalent cooling capacity. Figure 13 shows the simulation results for the average energy consumption of the conventional air conditioner and newly-developed solar-assisted air conditioning systems during the summer in the southern hemisphere. It can be seen that the power consumption of new solar-assisted air conditioner is significantly less than the power usage of conventional plant. To show the energy saving potential, average COPs are compared between the newly-developed system and a conventional system of the same capacity by using both experimental and simulation data. They are shown in Fig. 14 for five successive months of a hot season of the year in the southern hemisphere. It can be seen that the average COP for the proposed system is higher than that of a conventional one. This COP improvement can be explained by the new system's capability of energy saving with respect to the cooling demand, which coincides with the results presented in Fig. 13.

4.3 Effect of Varying Parameters

The overall thermal performance of the system is influenced by such operation parameters as the storage tank average water temperature, storage tank volume and room set-point temperature. The effect of the monthly average water temperature of the storage tank on the percent of energy saving is

shown in Fig. 15. From this figure, it is obvious that increasing the storage temperature can result in higher energy efficiency. On other hand, increasing the solar radiation intensity would increase the building cooling load and also the water temperature inside the storage tank. Simulation results show that the influence of the solar radiation intensity on raising the water temperature is more significant than that on cooling load. Thus, with a higher solar radiation level, more electricity savings can be expected.

Figure 16 shows the variation of the system energy consumption as a function of the water storage tank volume for summer, where it can be seen that with the increasing storage tank volume, the electricity power consumption decreases initially but tends to reach a minimum value asymptotically. It is interesting to note that the storage tank volume greater than38Ldoes not have much influence on the system energy usage. Furthermore, the effect of tank volume of less than 15 L is not noticeable, in terms of energy savings. However, for a given collector area with its tank volume, as the room temperature achieves its desired set-point, the refrigerant entering the evaporator is able to absorb heat from the circulated air. During this period, the compressor still remains off and the high temperature refrigerant leaving the hot water storage tank goes directly through the condenser. An additional refrigerant temperature taken by the storage tank then helps the compressor to stay off longer. The frequent turning off repetition of the compressor prevents full utilization of electricity resource potential and leads to a higher system efficiency. Therefore, the monthly average coefficient of performance can be overall increased. Moreover, an increase in the room set-point temperature can also result in an amount of the electric power saving, as expected. This is illustrated in Fig. 17showing the variation of the system's average power consumption with the room air temperature for each summer month.

5. Conclusion

This paper has presented the derivation of component-wise models and their simulation-experimental validation for predicting the operational performance and energy consumption of a new hybrid solar-assisted air-conditioning system. The models are derived based on the mass and energy balance

equations incorporating thermodynamics and heat transfer laws. Simulation results were compared with experimental data collected from a test rig equipped with sensors and data logging devices for validation of the mathematical models. Results verify sufficient accuracy of the derived models for predicting the system performance. A computer model based on TRNSYS is developed to predict how changes in system parameters would affect the performance in terms of energy saving and consumption. It is shown that additional heat from solar collectors to the refrigerant after the compressor allows it to be switched off longer to consequently reduce the overall electrical energy consumption. To reject the additional heat amount obtained from the water storage tank, a slightly larger condenser is used. With not much change in the manufacturing cost, the effect of the condenser size on the energy consumption is analysed to show the system's overall cost effectiveness. The novel design is promising for increasing of the system average energy efficiency while fulfilling the cooling demand with a higher coefficient of performance. The proposed hybrid solar air-conditioner can save between 25% and 42% of monthly average electricity.

Acknowledgements

This work is supported, in part, by The New South Wales Government through its Environmental Trust, Grant 2012/RDS034 and by a UTS Distinguished Visiting Scholar scheme.

References

[1] J.P. Praene, O. Marc, F. Lucas and F. Miranville,Simulation and experimental investigation of solar absorption cooling system in Reunion Island,Applied Energy,88 (2011) 831-839.

[2] W. Chen and S. Deng, Development of a dynamic model for a DX VAV air conditioning system, Energy Conversion and Management, 47 (2006) 2900-2924.

[3] X. Liang, M.Y. Chan, D. Shiming, and X. Xiangguo, Dehumidification effects in the superheated region (SPR) of a direct expansion (DX) air cooling coil, Energy Conversion and Management, 50 (2009) 3063-3070.

[4] C.H. Liang, X.S. Zhang, X.W. Li and X. Zhu, Study on the performance of a solar assisted air source heat pump system for building heating, Energy and Buildings, 43 (2011) 2188-2196.

[5] V. Vakiloroaya, Q.P. Ha and B. Samali, Energy-efficient HVAC systems: Simulation-empirical modeling and gradient optimization, Automation in Construction, 31 (2013) 176-185.

[6] C.F.A. Afonso, Recent advances in building air conditioning systems, Applied Thermal Engineering, 26 (2006) 1961-1971.

[7] K.F. Fong, T.T. Chow, C.K. Lee, Z. Lin and L.S. Chan, Comparative study of different solar cooling systems for buildings in subtropical city, Solar Energy, 84 (2010) 227-244.

[8] S.A. Kalogirou, Solar thermal collectors and applications, Progress in Energy and Combustion Science, 30 (2004) 231-295.

[9] R.Z. Wang and X.Q. Zhai, Development of solar thermal technologies in China, Energy, 35 (2010) 4407-4416.

[10] M. Thirugnanasambandam, S. Iniyan and R.Goic, A review of solar thermal technologies, Renewable and Sustainable Energy Reviews, 14 (2010) 312-322.

[11] S. Bergero and Anna Chiari, On the performance of a hybrid air-conditioning system in different climatic conditions, Energy, 36 (2011) 5261-5273.

[12] J. Jeon, S. Lee, Daehie Hong and Y. Kim, Performance evaluation and modeling of a hybrid cooling system combining a screw chiller with a ground source heat pump in a building, Energy, 35 (2010) 2006-2012.

[13] Q. Ma, R.Z. Wang, Y.J. Dai and X.Q. Zhai, Performance analysis on a hybrid air-conditioning system of a green building, Energy and Buildings, 38 (2006) 447-453.

[14] Z. Sagia, C. Rakopoulos and E. Kakaras, Cooling dominated hybrid ground source heat pump system application, Applied Energy, 94 (2012) 41-47.

[15] M. Bilgili, Hourly simulation and performance of solar electric-vapor compression refrigeration system, Solar Energy, 85 (2011) 2720-2731.

[16] B.J. Huang, J.H. Wu, H.Y. Hsu and J.H. Wang, Development of hybrid solar-assisted cooling/heating system, Energy Conversion and Management, 51 (2010)1643-1650.

[17] A. Al-Alili, Y. Hwang, R. Radermacher and L. Kubo, A high efficiency solar air conditioner using concentrating photovoltaic/thermal collectors, Applied Energy, 93 (2012) 138-147.

[18] Q. Ha, Data acquisition, monitoring and control for hybrid solar air-conditioners,Gerontechnology, 11 (2012)314.

[19] Q.P. Ha and V. Vakiloroaya, A novel solar-assisted air-conditioner system for energy savings with performance enhancement,Procedia Engineering, 49 (2012) 116-123.

[20] TRNSYS software, A transient system simulation program, version 16 (2006),Wisconsis-Madison University. Available: http://sell.me.wisc.edu/trnsys/.

[21] G. Diaz, Controllability of cross-flow two-phase heat exchangers, International Journal of Heat and Mass Transfer, 50 (2007) 4559-4567.

[22] ANSI/ASHRAE Standard 140, Standard Method of Test for the Evaluation of Building Energy Analysis Computer Program, American Society of Heating, Refrigerating and Air-Conditioning, 2007.

[23] V. Vakiloroaya, R. Dibbs, Q.P. Ha and B. Samali, Hybrid solar air conditioner modelling and optimal usage for energy usage and comfort enhancement, Proc. The Second International Conference on Building Energy and Environment (COBEE), Boulder, Colorado, (2012) 711-718.

Figure Captions

Fig. 1. Schematic diagram of the solar-assisted air conditioner system

Fig. 2.Schematic of the evaporator model

Fig. 3.Schematic of the condenser model

Fig. 4. Photograph of the experimental system

Fig. 5. Simulation flow chart in TRNSYS work space

Fig. 6. Predicted and experimental temperature of refrigerant leaving the evaporator

Fig. 7. Predicted and experimental temperature of refrigerant leaving the compressor

Fig. 8. Predicted and experimental temperature of refrigerant leaving water storage tank

Fig. 9. Predicted and experimental temperature of refrigerant leaving condenser

Fig. 10. Predicted and experimental temperature of water in storage tank

Fig. 11. Predicted and experimental temperature of refrigerant leaving capillary tube

Fig. 12.Monitored experimental data for ambient temperature and humidity

Fig. 13. Energy consumption comparison

Fig. 14.Coefficient of performance (COP) comparison

Fig. 15. Energy saving potential versus average storage tank water temperature

Fig. 16. Variation of system energy consumption versus storage tank volume

Fig. 17. Variation of system power consumption versus room set-point temperature

Table Captions

Table 1.Main parameters used in the model validation and performance prediction of the HSAC system

Table 2. Statistical characteristics

Table 1. Main parameters used in the model validation and performance prediction of the HSAC system

Evaporator outer diameter of tubes (D_{eo})	12.7 mm
Evaporator inner diameter of tubes (D_{ei})	11.8 mm
Evaporator fin-to-fin area (A_e)	0.17 m^2
Evaporator total length (L_e)	0.9 m
Evaporator two phase heat transfer coefficient ($\alpha_{i,e,tp}$)	2 kW/m^2°C
Evaporator superheated heat transfer coefficient ($\alpha_{i,e,sh}$)	0.31 kW/m^2°C
Evaporator external heat transfer coefficient ($\alpha_{o,e}$)	0.48 kW/m^2°C
Condenser outer diameter of tubes (D_{co})	9.5 mm
Condenser inner diameter of tubes (D_{ci})	8.6 mm
Condenser fin-to-fin area (A_c)	0.52 m^2
Condenser total length (L_c)	0.8 m
Condenser de-superheated heat transfer coefficient ($\alpha_{i,c,ds}$)	0.25 kW/m^2°C
Condenser two phase heat transfer coefficient ($\alpha_{i,c,tp}$)	2 kW/m^2°C
Condenser superheat heat transfer coefficient ($\alpha_{i,c,sh}$)	0.24 kW/m^2°C
Condenser external heat transfer coefficient ($\alpha_{o,c}$)	0.3 kW/m^2°C
Water storage tank area(A_t)	1.6 m^2
Vacuum solar collector area (A_{col})	1.9 m^2
Tank immersed coil area (A_{hx})	0.11 m^2
Tank heat loss coefficient (U_t)	0.3 kW/m^2°C
Immersed coil heat loss coefficient (U_{hx})	0.12 kW/m^2°C
Collector transmittance value (τ_s)	0.91
Collector absorptance value (α_s)	0.92
Specific heat of refrigerant ($C_{p,r}$)	1.13 kJ/kg °C
Specific heat of water ($C_{P,f}$)	4.2 kJ/kg °C
Water mass in storage tank (M_f)	35Kg
Displacement volume of compressor (V_D)	0.0012 m^3/sec
Volumetric efficiency (η_v)	0.91
Polytropic index of R410A (k)	1.17
Total efficiency of the compressor (η_{comp})	0.8

Table 2. StatisticalCharacteristics

Parameter	$y_{data,m}$	s_x	RE	RMSE	VC
$T_{r,o,e}$	16.68	3.22	9.57%	1.73	10.37%
$T_{r,o,comp}$	53.11	9.21	11.4%	6.25	11.77%
$T_{r,o,t}$	61.2	9.59	12.18%	7.38	12.97%
$T_{r,o,c}$	30.03	2.57	12.38%	3.95	13.15%
$T_{r,o,cap}$	11.39	3.58	9.49%	1.13	9.97%
T_f	80.75	4.45	10.98%	9.31	11.53%

Figure(s)

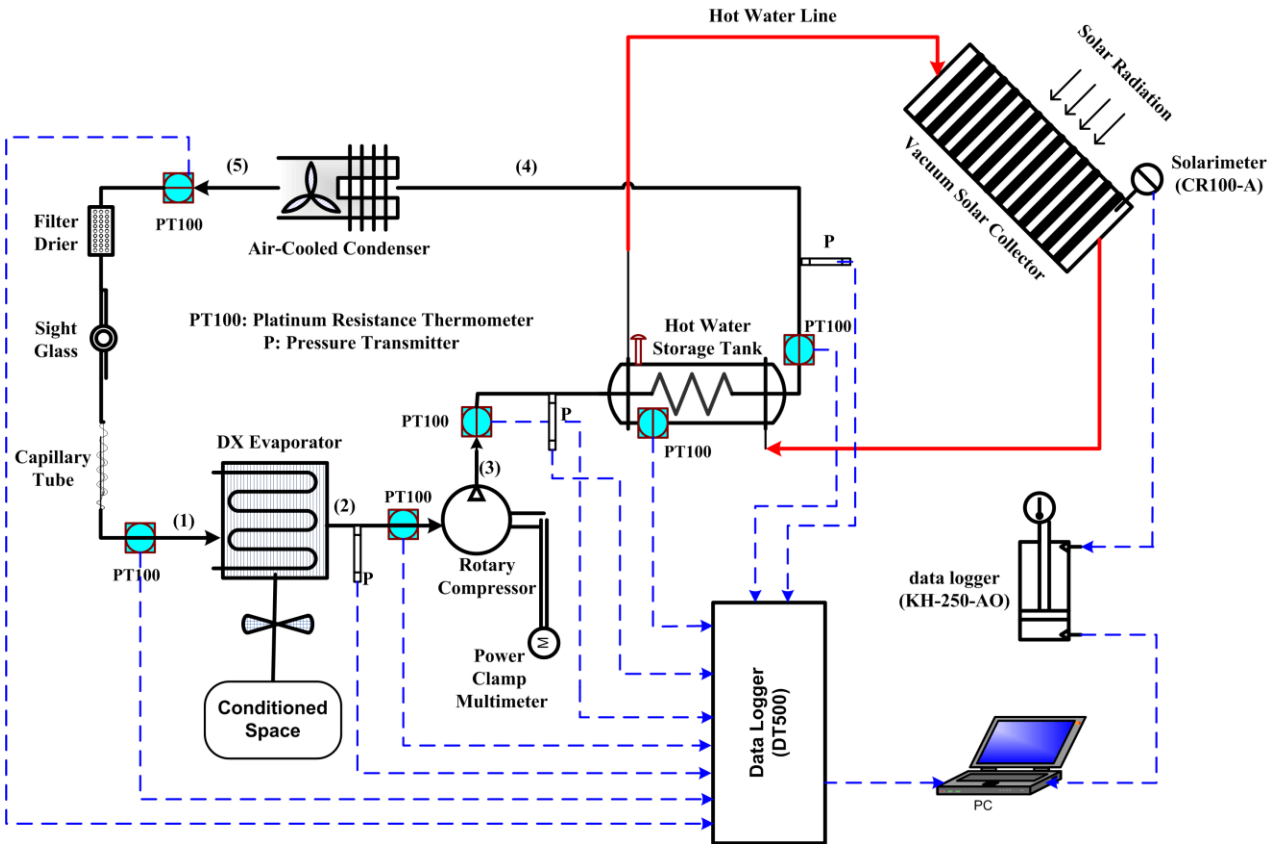

Fig. 1. Schematic diagram of the solar-assisted air conditioner system

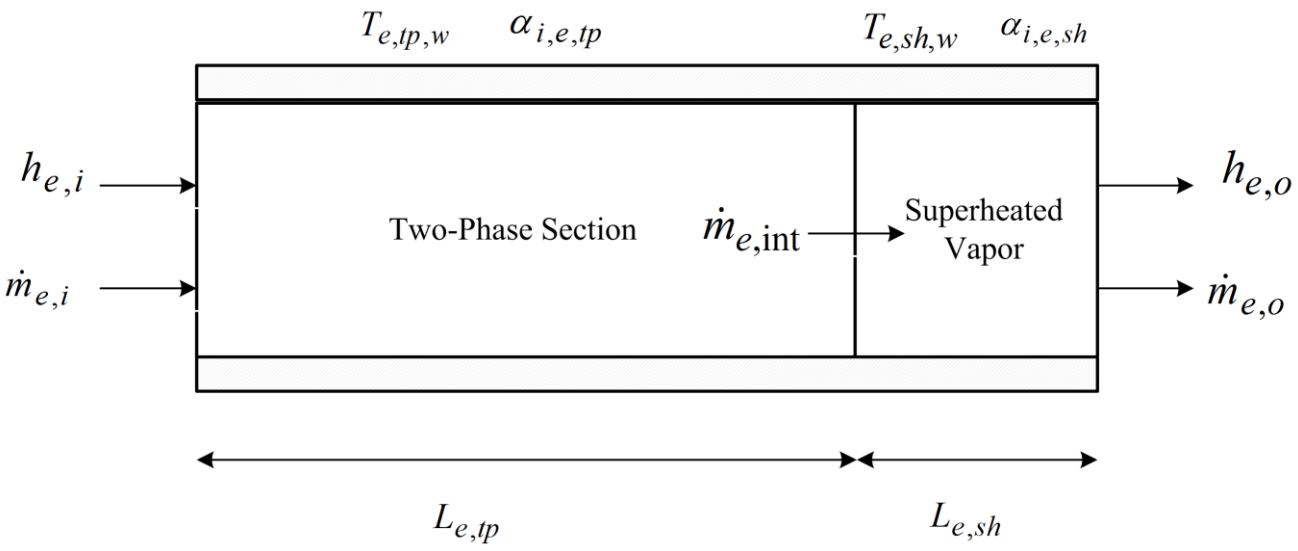

Fig. 2. Schematic of the evaporator model

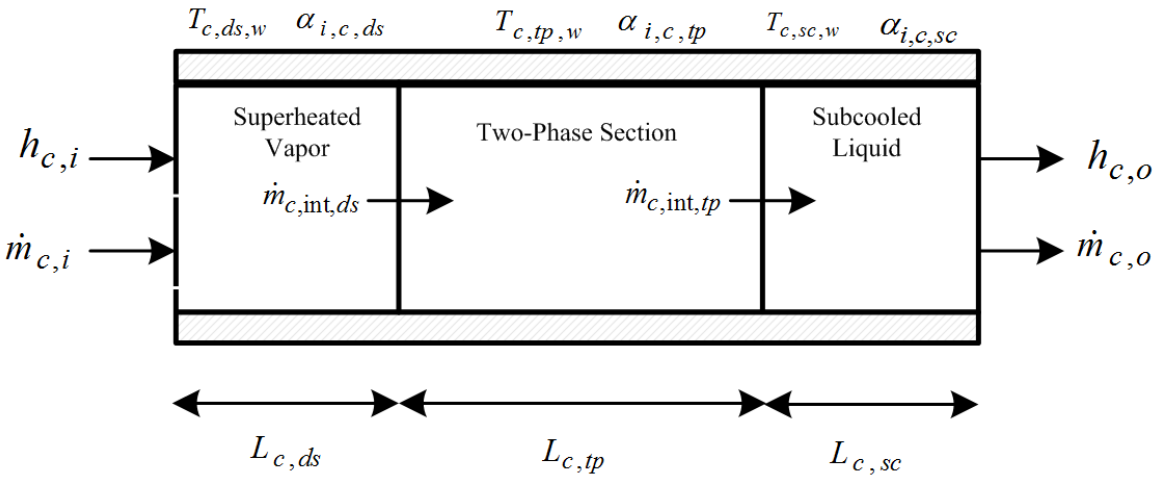

Fig. 3. Schematic of the condenser model

Fig. 4. Photograph of the experimental system

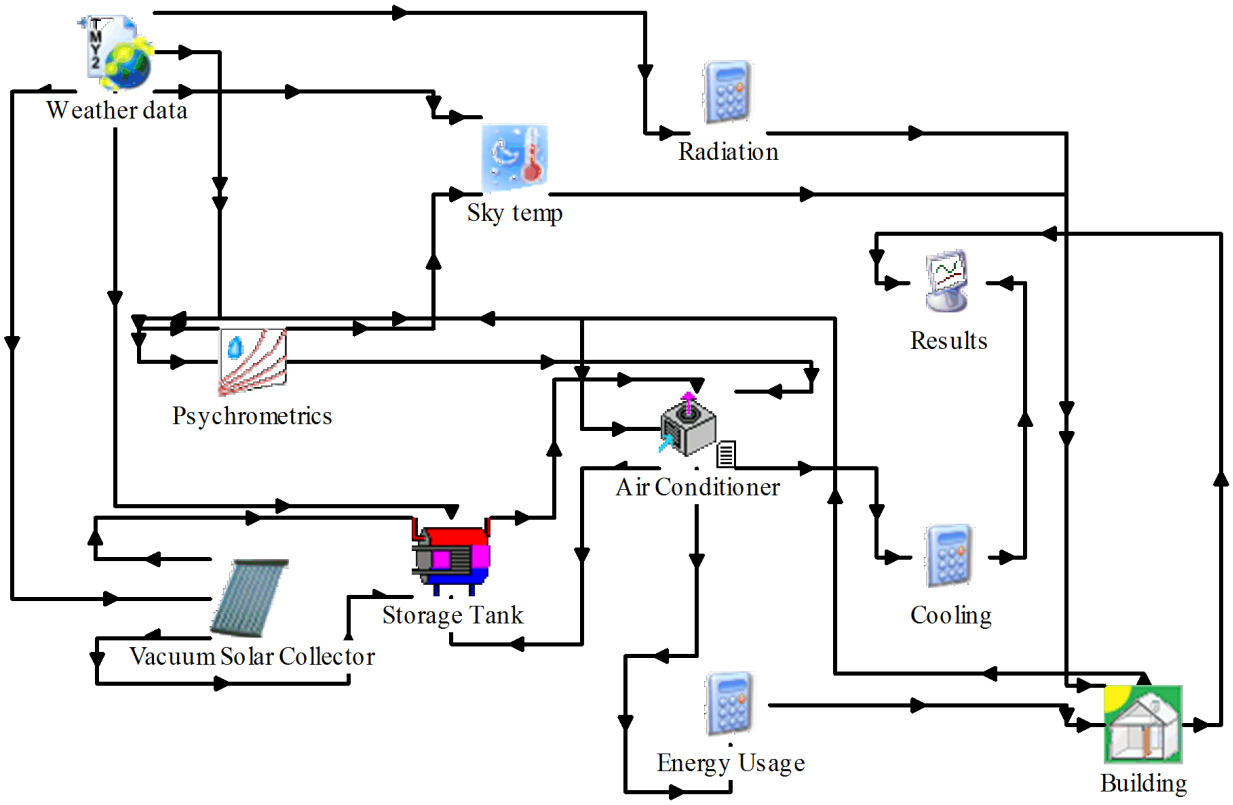

Fig. 5. Simulation flow chart in TRNSYS work space

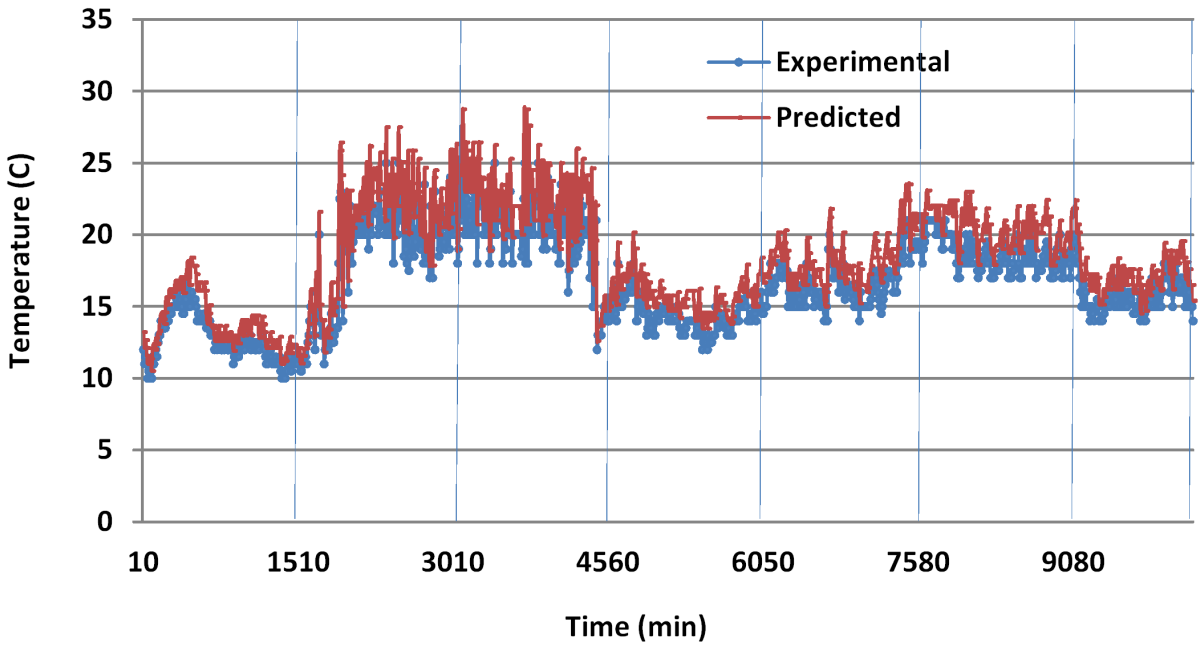

Fig. 6. Predicted and experimental temperature of refrigerant leaving the evaporator

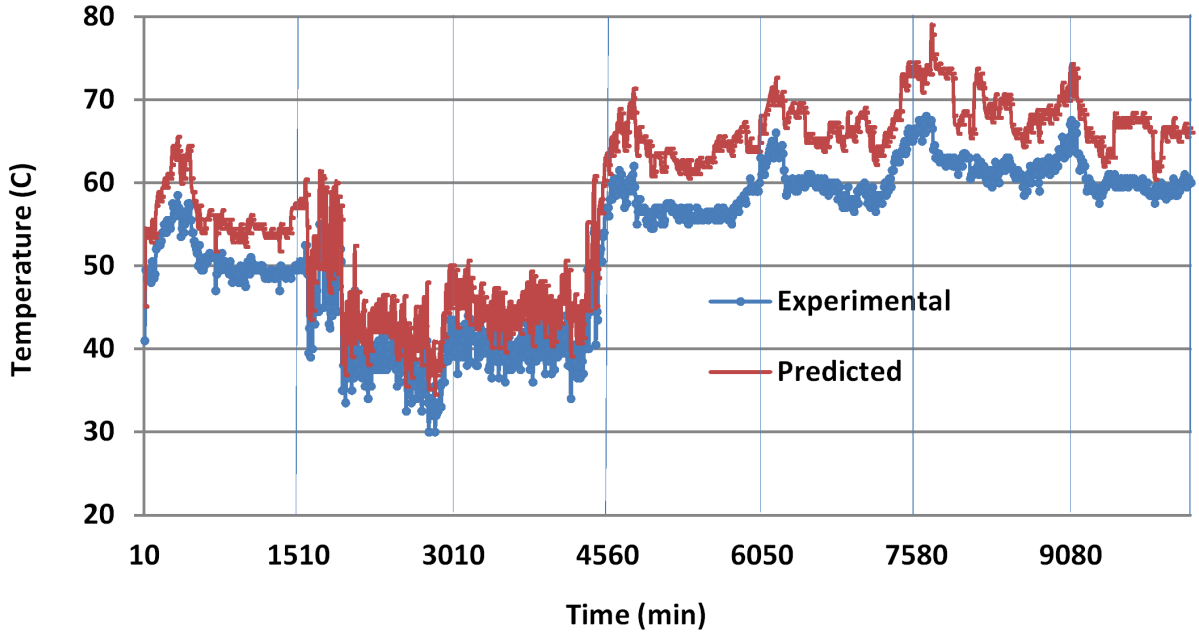

Fig. 7. Predicted and experimental temperature of refrigerant leaving the compressor

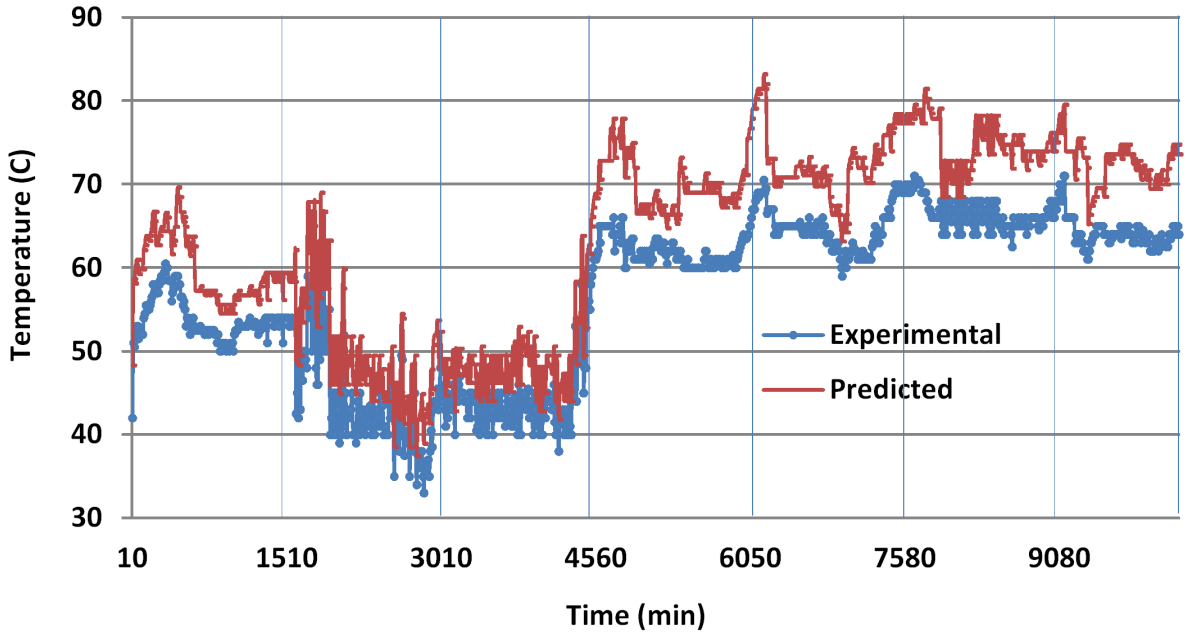

Fig. 8. Predicted and experimental temperature of refrigerant leaving water storage tank

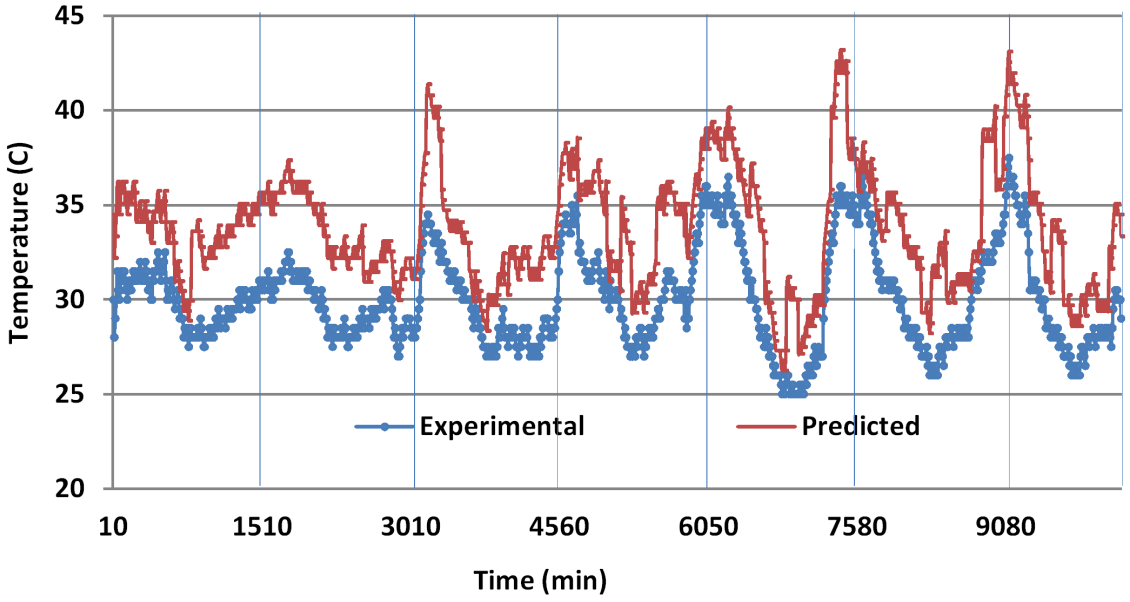

Fig. 9. Predicted and experimental temperature of refrigerant leaving condenser

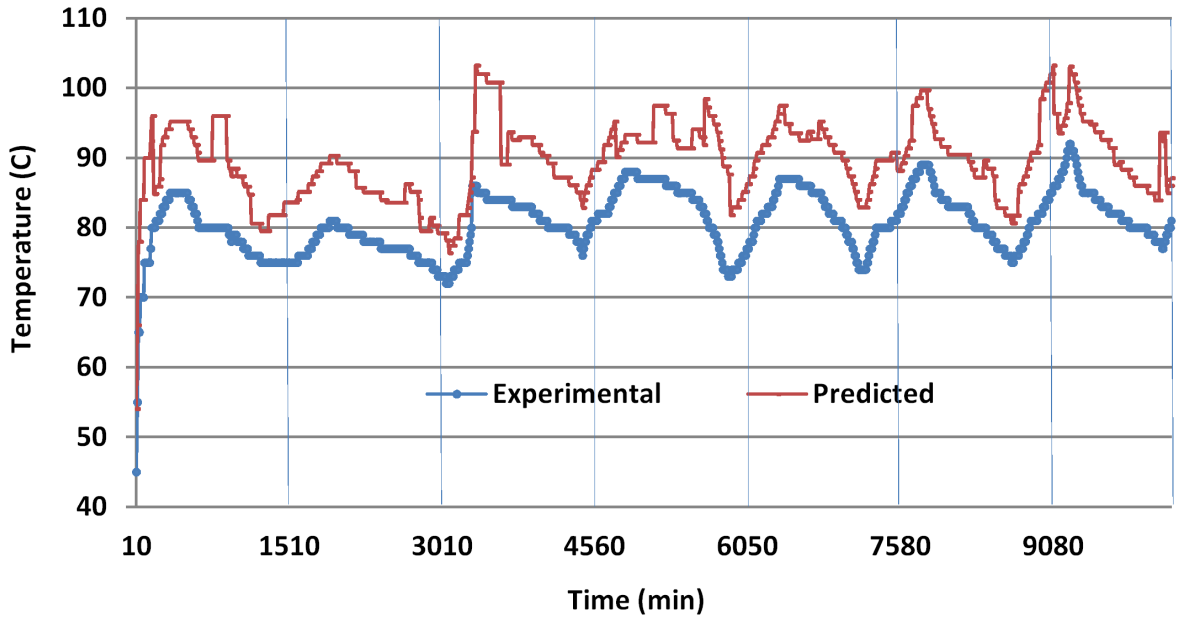

Fig. 10. Predicted and experimental temperature of water in storage tank

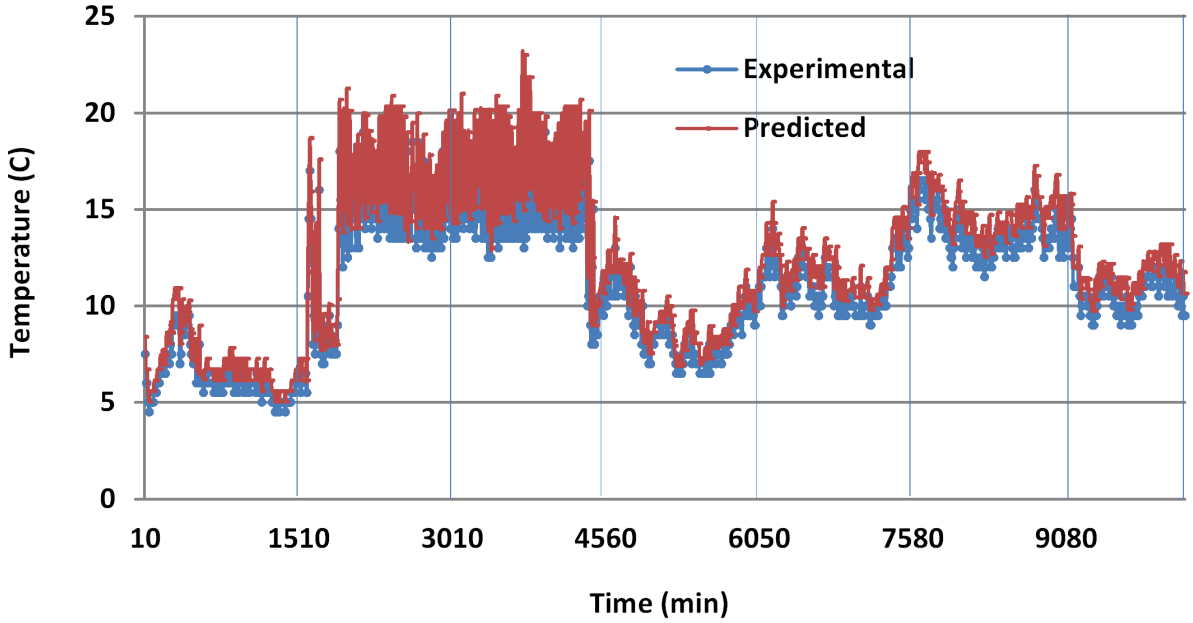

Fig. 11. Predicted and experimental temperature of refrigerant leaving capillary tube

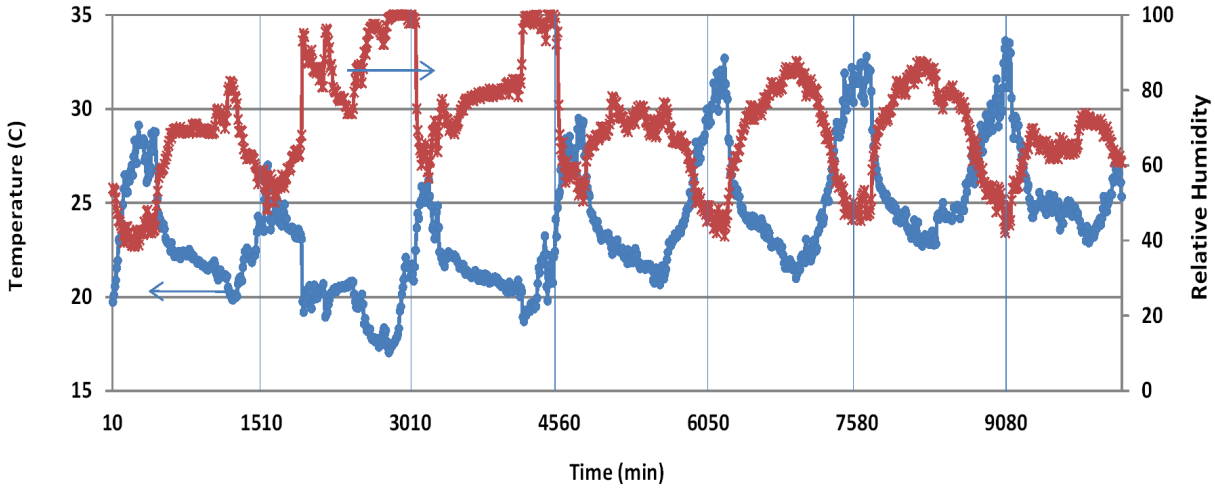

Fig. 12. Monitored experimental data for ambient temperature and humidity

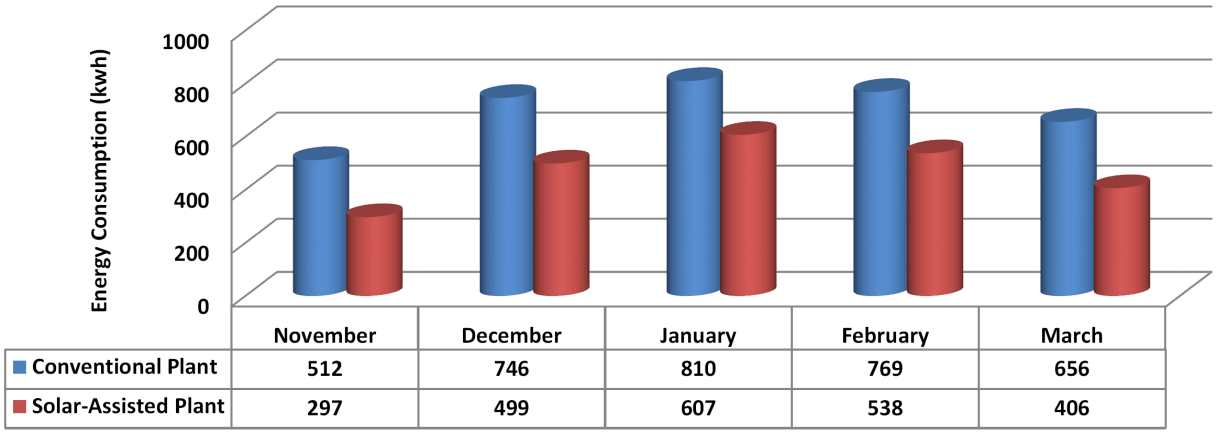

	November	December	January	February	March
Conventional Plant	512	746	810	769	656
Solar-Assisted Plant	297	499	607	538	406

Fig. 13. Energy consumption comparison

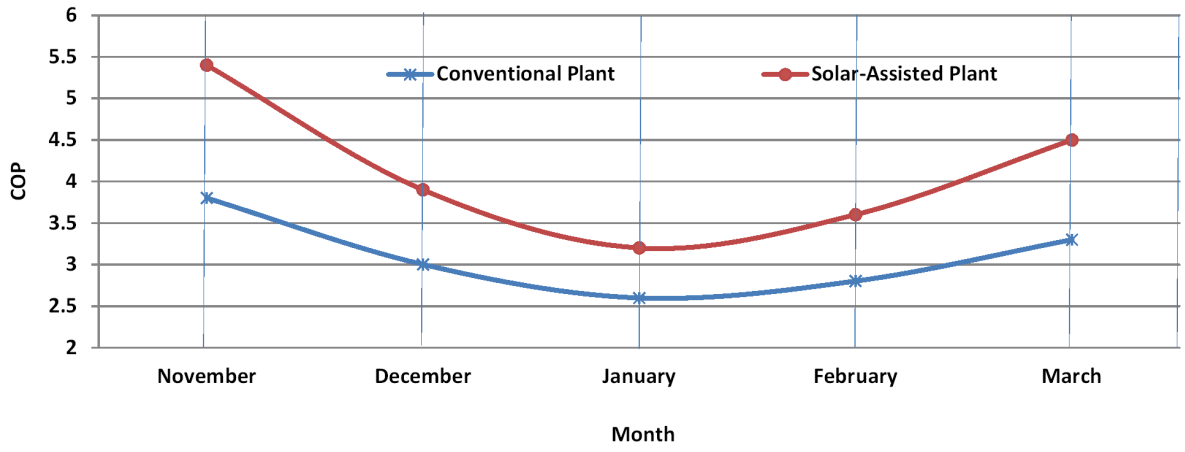

Fig. 14. Coefficient of performance (COP) comparison

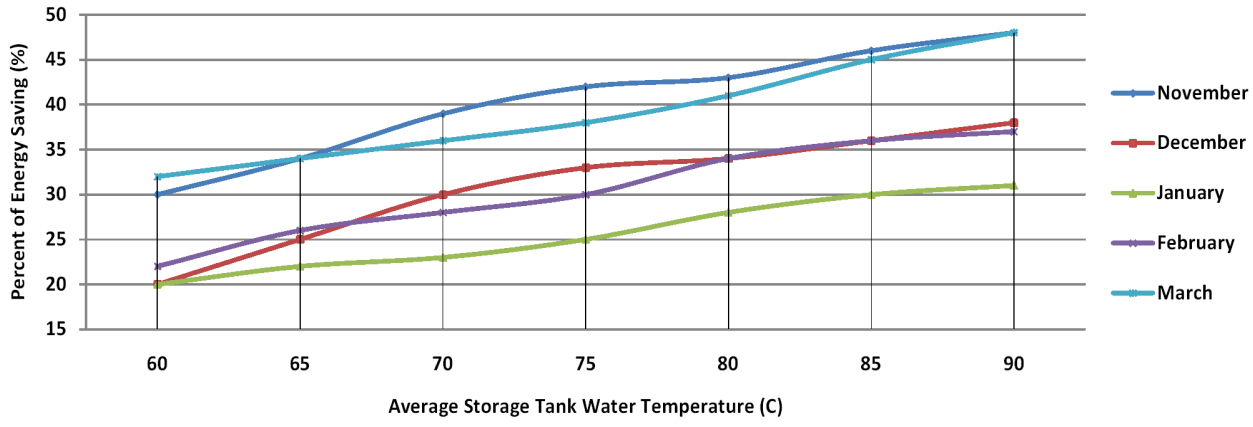

Fig. 15. Energy saving potential versus average storage tank water temperature

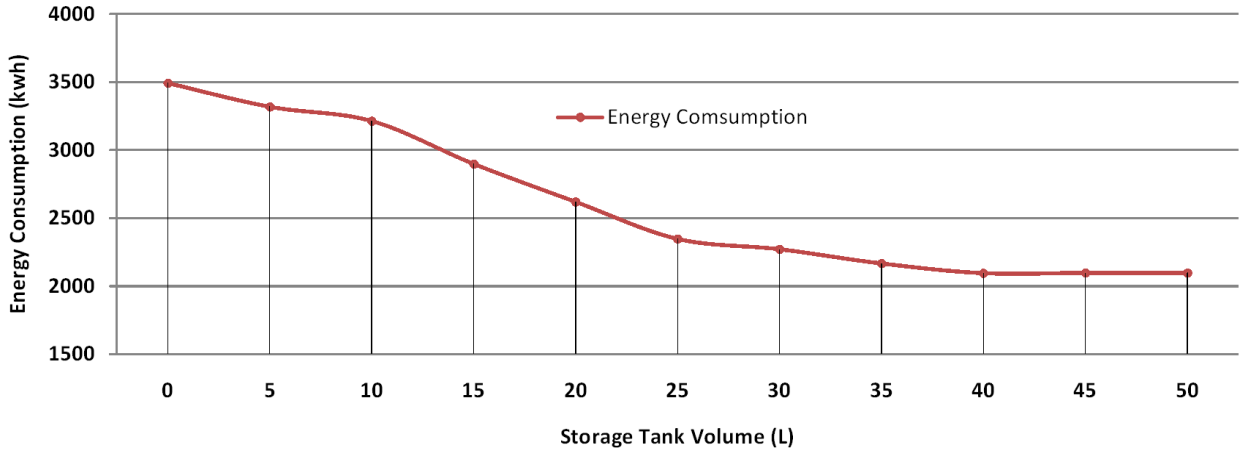

Fig. 16. Variation of system energy consumption versus storage tank volume

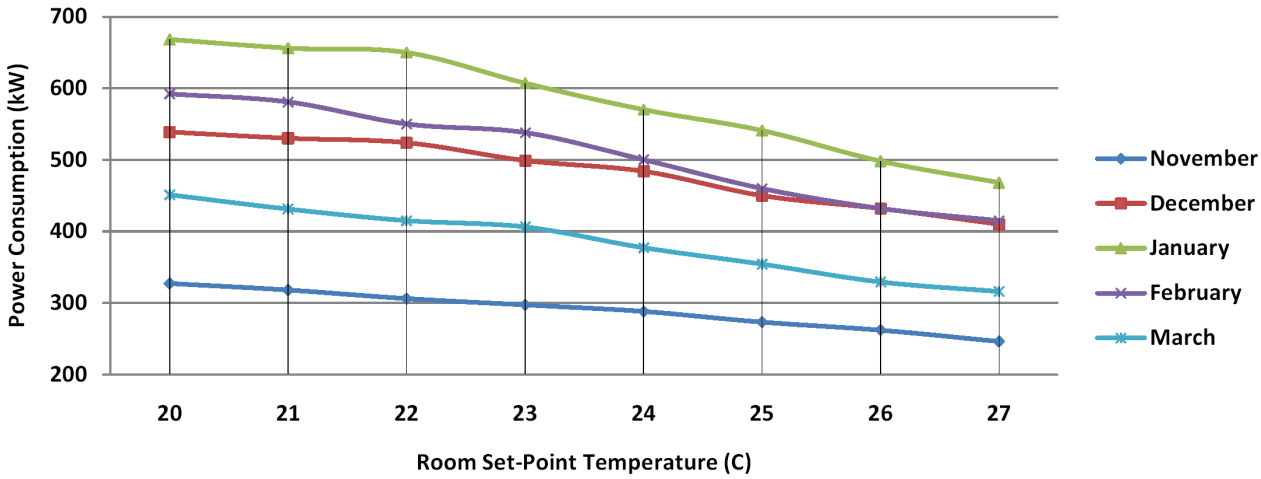

Fig. 17. Variation of system power consumption versus room set-point temperature

Highlights

- Derivation of component-wise models for performance prediction.
- Field tests conducted for a new solar-assisted air conditioning system.
- Model verification by using experimental data and algorithms implemented in TRNSYS.
- Between 25% and 42% monthly average energy saving while fulfilling cooling demand.